Title

Accomplishments and challenges in stem cell imaging in vivo.

Journal

Drug discovery today, 24(2)

ISSN

1359-6446

Authors

Bose, Rajendran JC
Mattrey, Robert F

Publication Date

2019-02-01

DOI

10.1016/j.drudis.2018.10.007

Peer reviewed

Teaser Advances in molecular imaging have led to extraordinary progress, with several strategies being deployed to understand the fate of stem cells in vivo. This review provides a comprehensive and timely overview of recent advances, challenges and future perspectives of different imaging modalities used in stem cell tracking and functional assessment.

Accomplishments and challenges in stem cell imaging *in vivo*

Rajendran J.C. Bose[1,2] and Robert F. Mattrey[1]

[1] Department of Radiology and Advanced Imaging Research Center, 5323 Harry Hines Blvd, UT Southwestern Medical Center, Dallas, TX 75390-8514, USA
[2] Current affiliation: Molecular Imaging Program at Stanford (MIPS) and the Canary Center at Stanford for Cancer Early Detection, Department of Radiology, School of Medicine, Stanford University, Stanford, CA 94305-5427, USA

Stem cell therapies have demonstrated promising preclinical results, but very few applications have reached the clinic owing to safety and efficacy concerns. Translation would benefit greatly if stem cell survival, distribution and function could be assessed *in vivo* post-transplantation, particularly in patients. Advances in molecular imaging have led to extraordinary progress, with several strategies being deployed to understand the fate of stem cells *in vivo* using magnetic resonance, scintigraphy, PET, ultrasound and optical imaging. Here, we review the recent advances, challenges and future perspectives and opportunities in stem cell tracking and functional assessment, as well as the advantages and challenges of each imaging approach.

Introduction

The landscape of stem cell (SC) therapy has changed dramatically in recent years [1]. SCs of embryonic (ESCs) [2], mesenchymal (MSCs) [3] and neuroprogenitor (NSCs) origin [4], as well as induced pluripotent stem cells (iPSCs) [2,5,6], have garnered increased attention owing to their therapeutic and regenerative potential. SCs have been used to treat diverse diseases such as Parkinson's disease [7] and liver disease [8], as well as to repair ischemic and infarcted tissues [9], including acute myocardial infarction [10]. Efficacy of SC therapy has generally relied upon *ex vivo* genetic manipulation or modifications using cytokines or small molecules [11], which alter SC function and behavior profile; however, these changes can also induce unwanted side effects [12]. Therapeutic efficacy depends on several factors such as SC origin and source, route of administration, biodistribution, cell survival after transplantation, as well as the disease itself [12,13]. The ability to confirm SC accumulation in their intended target tissue, define acute and long-term viability and desired function, determine their accumulation in non-desired locations and assess their interaction with the host in a noninvasive manner would greatly enhance their safety and efficacy [14,15]. Labeling SCs with reporters or reporter genes to enable their detection and assess their function *in vivo* has been achieved using all current imaging modalities with promising preclinical results, and with some success in clinical trials [16]. However, at present, there is no

Corresponding author: Mattrey, R.F. (Robert.Mattrey@UTSouthwestern.edu)

Rajendran J.C. Bose received his BS and MS degrees in pharmacy from Tamil Nadu Dr MGR Medical University (Chennai, India) in 2009; and received his PhD in bioengineering from Chung – Ang University (Seoul, South Korea), in collaboration with the CHA stem cell institute (Seongnam, South Korea) in 2016. He joined Dr Robert Mattrey at UT Southwestern as a postdoc after his PhD, and is currently performing a second postdoc with Professor Ramasamy Paulmurugan at Stanford University. His research interests are translational molecular imaging, nanomedicine, cell therapy and cancer immunotherapy.

Robert F. Mattrey is Professor of Radiology and the Advanced Imaging Research Center (AIRC) at UT Southwestern and is an Established Investigator and CPRIT Scholar. He received his bachelor's and master's degrees in electrical engineering and his medical degree from the State University of New York at Buffalo. He completed his residency training in diagnostic radiology and completed fellowship training in X-ray computed tomography, ultrasound and interventional radiology at the University of California, San Diego. Dr Mattrey's research is in contrast media in general and molecular imaging in particular, with emphasis on ultrasound solutions. He has translated several agents from concept, through preclinical safety and efficacy and to clinical trials over his career.

https://doi.org/10.1016/j.drudis.2018.10.007

ideal imaging approach, each having advantages and limitations. This review presents the approaches and achievements made with each imaging modality, as well as advantages, limitations and challenges for translation. We will highlight future advances in SC imaging and present potential opportunities for image-guided therapeutic intervention.

SC labeling techniques

Advances in SC labeling, imaging and tracking have enabled longitudinal monitoring *in vivo*, as well as assessment of viability and function [12], mostly in preclinical studies [17]. Direct or indirect labeling of SCs with molecular probes has been achieved with advantages and disadvantages to each approach [14,17]. Direct labeling involves the loading of SCs before engrafting with a sufficient amount of reporters to enable their detection with the imaging modality of choice. Although sufficient reporter concentration enables SC imaging at the desired spatial and temporal resolution, it suffers from several challenges, the most important of which are reporter dilution as cells divide and migrate, reporter rather than SC tracking and difficulty in assessing SC viability and function. Indirect labeling involves the incorporation of a reporter gene within SCs that require transfection with either viral or nonviral carriers as well as sufficient transfection efficiency to detect the expressed reporters when engrafted. Because the introduced gene can only be expressed by live cells its detection infers cell viability. Many reporter genes have been proposed, where the expressed protein can be imaged directly, such as florescent proteins [18], can trap iron to become detectable [19], can be used as a receptor to target reporters [20] or can be an enzyme that induces reporter trapping [21], or converts an invisible to a visible reporter [22]. Although reporter genes overcome some of the challenges of direct labeling, they have challenges of their own. Unless the gene is incorporated within the genome, it has limited survival time, and also suffers from dilution effects with cell division and migration, albeit less than direct reporter labeling. Further, the transfection strategy, particularly if viral vectors are used, and if the expressed protein reaches the extracellular space, raises concern of mutagenesis, toxicity and immune and allergic responses (Fig. 1)

Overview of SC imaging technologies

All imaging modalities have been attempted with a degree of success for each approach dependent on the reporter used, labeling strategy, cell concentration required for detection, spatial resolution, imaging time and the application itself. Advantages and limitations of each approach are summarized in Table 1. At any

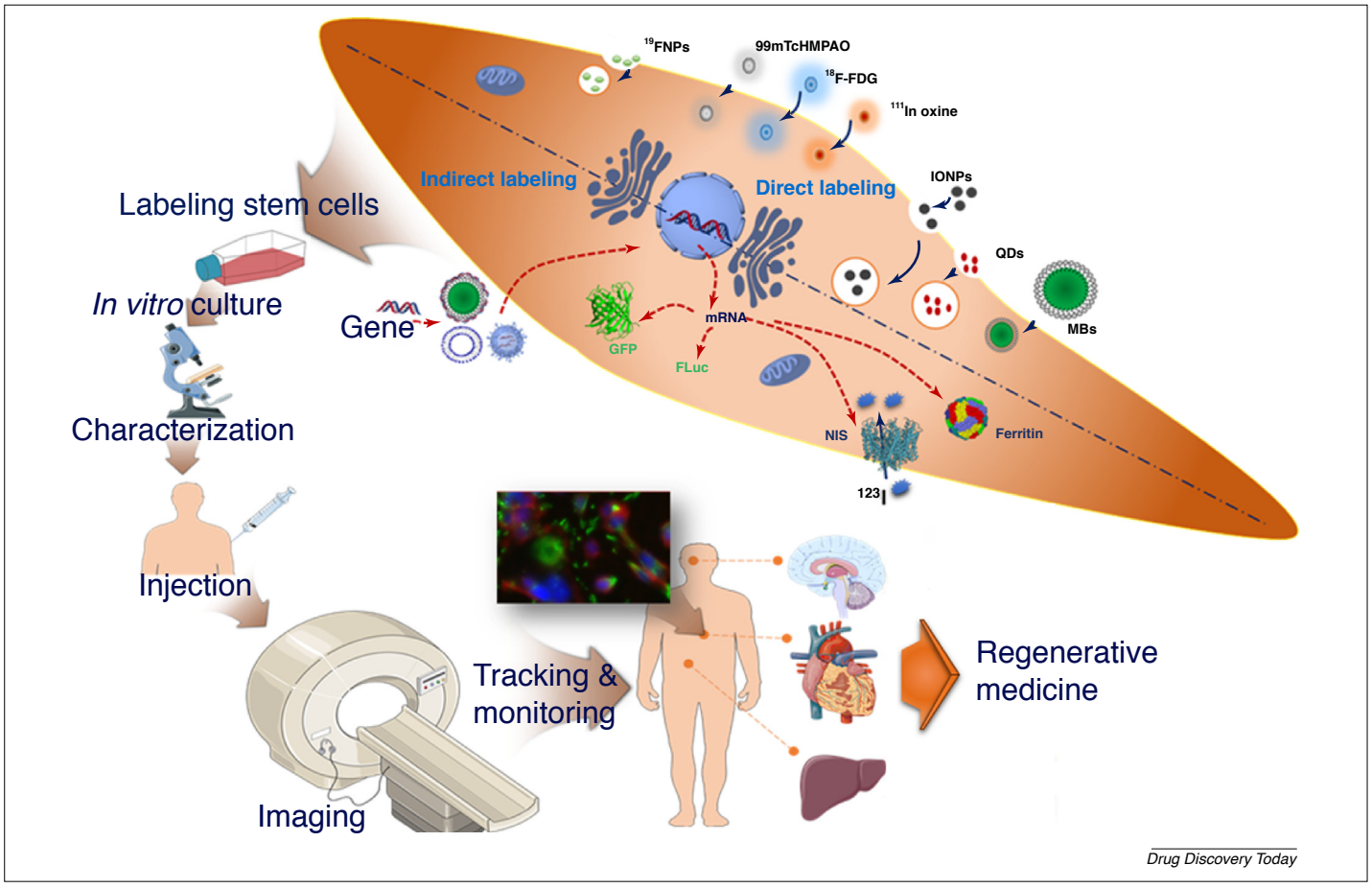

FIGURE 1

Cartoon summarizing various direct and indirect labeling strategies and the use of stem cells in regenerative medicine. Composite illustrations to build the cartoon were in part adopted from Servier Medical Art by Servier (https://smart.servier.com). Original images are licensed under a Creative Commons Attribution 3.0 Unported License.

TABLE 1

Summary of characteristics, reporters used and advances and limitations of each proposed stem cell *in vivo* imaging technique

Imaging methods	Contrast agents	Acquisition time	Spatial resolution	Minimum cells #/voxel detected *in vivo*	Method suitability	Advantages	Limitations
PET	• F-18 (FDG, FHBG, FDOPA) • 64Cu-PTSM • Sodium iodide symporter (NIS) • HSV1-tk + F-18 acycloguanosine or pyrimidine analog	Seconds to minutes	>1–2 mm	~10 000 cells	Preclinical and clinical	• 3D imaging • High sensitivity • High labeling efficiency • Able to image deep tissues • Used clinically	• Expensive • Low spatial resolution • Anatomic reference required • Concern for radiation dose
SPECT	• 99mTc-HMPAO • In-111 • Sodium iodide symporter (NIS) • Dopamine receptor • HSV1-tk	Minutes	>1–2 mm	~100 000 cells	Preclinical and clinical	• 3D imaging • Can use multiple reporters • Preferable method for large animal studies • Used clinically	• Limited spatial resolution • Quantification is challenging • Concern for radiation dose
MRI	• Iron oxide nano- micro-particles • Gd chelates, Gd oxide NPs • F-19 – perfluorocarbons • Si-Gold NPs • Metalloproteins • Metal ion transporters • Water channel aquaporin • Lysine-rich protein	Minutes to hours	Resolution scales with RF coil, imaging time and reporter concentration (from 50 μm to 5 mm)	~10 000 cells	Preclinical and clinical	• Excellent tissue contrast • Nonionizing • Quantitative • Long-term imaging ability (<1 month)	• Expensive • Complex procedure • Not all patients can be imaged
US	• Gas filled MBs • Detects endothelial cell gene expression with targeted MBs • Microcapsules • Liposomes	Real-time	Resolution scales with frequency (50 μm at <1 cm, to 1–2 mm at 15–20 cm)	1–10 cells	Preclinical and clinical	• Extremely high sensitivity • Real-time imaging to 20 cm depth of field • Inexpensive, nonionizing, and portable • Most common imaging tool worldwide • Used for image-guided stem cell grafting	• limited 3D capabilities • Limited quantification • Not suitable for lung imaging • Limited intracranial imaging
CT	• Microcapsules • Barium • Gold nanoparticles	Seconds to minutes	High resolution 20 μm in mice, <1 mm in human	Unknown	Preclinical and clinical	• 3D imaging • Relatively inexpensive • High resolution	• Very poor sensitivity • Uses ionizing radiation
BLI	• Chemiluminescent luciferase reactions	<1 minute	1–20 mm depending on depth of signal	~1000 cells	Preclinical	• Less expensive • High-throughput method • More suitable for long-term imaging in small animal studies	• Poor tissue penetration • Low *in vivo* resolution • Requires transfection of cells • Not suitable clinically
FLI	• Fluorescent dyes • Fluorescent polymeric NPs • Quantum dots (QDs) • Fluorescent proteins (GFP,RFP, . . .)	Real-time to seconds to minutes	1–10 mm depending on depth of field and signal	~1 000 000 cells	Preclinical and clinical	• Less expensive • Ideal for ultra-high resolution microscopy • Real-time	• Low resolution *in vivo* • Poor tissue penetration • Photobleaching • Tissue autofluorescence
PAI	• Optical absorbers	Real-time	<1 mm^3 depending on field of view	200–1000 cells	Preclinical and clinical	• Less expensive • Real-time • Higher resolution than US, FLI and BLI	• Limited penetration • Not suitable for brain or lung • Limited quantification
MPI	• Iron oxide nano- micro-particles	Seconds to minutes	≤1 mm^3	~10 000	Preclinical	• High contrast:noise ratio • Hotspot imaging	• Not yet available for large animal or human imaging • Same limitations as MRI • Requires multimodal imaging

given reporter concentration [number of reporters per voxel (the smallest detectable unit volume)], large voxels improve sensitivity (increase voxel signal), decrease noise [higher signal:noise ratio (SNR)] but also decrease spatial resolution. The higher the imaging sensitivity the fewer reporters per voxel are needed for detection and therefore the fewer SC per voxel that could be detected. Therefore, each imaging approach aims to detect the minimum number of SCs per voxel at the highest spatial resolution and shortest imaging time, which is challenged *in vivo* by the addition of motion that blurs images and decreases contrast:noise ratio (CNR).

Detection sensitivity *in vivo* is highest for optical fluorescence imaging (FLI) which can detect nanomolar concentrations with greater concentrations needed for bioluminescence imaging (BLI). This sensitivity is achieved at the expense of spatial resolution for *in vivo* imaging that is ~1 cm^3, and has extremely limited depth of penetration (<1 cm), because photons are highly scattered and attenuated in tissues. Further, photobleaching and background tissue fluorescence affect FLI, and data acquisition time and motion affect BLI. Although imaging with FLI is in real-time, BLI requires integration over time of emitted photons to reach an adequate SNR.

Positron emission tomography (PET) can detect at least a 100 nM concentration with slightly greater concentrations needed for single-photon emission computed tomography (SPECT). Low SNR, large voxel size and long imaging time (3–30 min) limit spatial resolution. In the case of PET, resolution is further compromised, because the characteristic dual photon emission that is captured by the detector ring occurs away from the nucleus of interest when the emitted positron interacts with an electron, which occurs at an unknown distance dependent upon positron energy. Distance travelled by the positron is the least for ^{18}F and is ~1 mm, defining a theoretical resolution limit of 1–2 mm voxel size.

MRI can detect T1 agents in the 10 μM range, and lesser concentrations for susceptibility (T2*) agents, such as iron oxide nanoparticles (IONPs). However, because the effect of T2* agents is signal loss, detection suffers from SNR limitations as well as poor specificity when tissues with short T2 are present in the imaged field. Some investigators have addressed poor IONP specificity by using ultra-short time to echo (TE) sequences to capture signal and recognize the T1 shortening effect of IONPs [23]; however, these pulsing sequences are not widely available. MRI SNR scales linearly with magnetic field strength, by the square root with imaging time, and radiofrequency (RF) coil type and size that captures signal with sufficient SNR at a desired depth. Under ideal optimized *in vitro* conditions, MRI can resolve a single IONP-labeled cell [24].

Magnetic particle imaging (MPI) is a newly described imaging technique that was first reported by Gleich and Weizenecker in 2005 [25]. Whereas MRI interrogates and detects signals from protons and the influence of contrast media on their behavior, MPI directly interrogates and detects signal from IONPs, where core size is ideally monodispersed and in the range of 20–40 nm. Because signal is only received from IONPs, images are analogous to nuclear imaging (tracer signal without background signal) or hotspot imaging, but signal is quantitative. Spatial resolution is slightly less than 1 mm^3. Signal is acquired 1 voxel at a time, and 2D or 3D volumes are acquired by raster scanning the voxel through the volume of interest. Raster scanning is the processing of sweeping the readout point through the volume of interest from right to left, anterior to posterior and superior to inferior. MPI sensitivity is expected to be slightly worse than PET imaging [25–29] but could be improved with instrument and formulation optimization. Its main limitation is that MPI requires new MR instruments, and has to date been limited to imaging mice and rats. MPI and its required IONP formulations will face significant challenges when translated to image human subjects.

X-ray computed tomography (CT) is the least sensitive modality. It requires mM concentrations for detection but boasts the highest spatial resolution of about 20 μm *in vivo* in small animals and ~100 μm in human subjects. SNR is dependent on radiation dose and reporter concentration.

As noted with all these techniques, as spatial resolution increases (CT > MR > SPECT > FLI) *in vivo* reporter sensitivity decreases. Ultrasound (US) stands alone in this regard. It provides high spatial resolution, exquisite sensitivity to its reporter: microbubbles (MB), and can do so with real-time imaging at the bedside. US spatial resolution scales with transmission frequency. It can resolve from tens of μm at 40–80 MHz down to 1–2 mm at 2 MHz. Unfortunately, the higher frequencies are highly attenuated, reaching depths of 1 cm at 40–80 MHz and 20 cm at 2 MHz. MBs of perfluorocarbon (PFC) vapor encapsulated in a phospholipid monolayer are 1–3 μm in diameter, are highly elastic and oscillate in the μm scale becoming strong US transmitters. The oscillations produce characteristic frequencies that allow the reconstruction of MB-only images allowing the detection of single MBs *in vitro* [30] and a single cell loaded with MBs *in vitro* and *in vivo* [31]. This exquisite sensitivity allows the use of miniscule diagnostic doses ~5×10^8 MBs that are administered in 0.1–1.0 ml total volume depending on the formulation. MB-specific US imaging is somewhat analogous to photoacoustic imaging (PAI), except that sound generation is accomplished with an ultrasound pulse and the point sources are the MBs in the insonated field. However, unlike PAI, MB-specific US imaging can reach >15 cm depth of field.

PAI has been introduced and made feasible in recent years. PAI transmits light into tissues that reach specific absorbers that heat, expand and cool rapidly, generating a soundwave detectable by an external array transducer. Detected sound is then used to generate an image of the point sources in the field of view. PAI is a hybrid technique that is more like optical imaging than US. The advantage of PAI over optical imaging is that light absorption that occurs deeper in tissues can be resolved because generated sound is not attenuated at these depths, and the time of arrival of US signal allows the distinction of the far field from near field signal. Further, because generated sound travels one-way from the point sources to the detector, the generated images have higher spatial resolution than standard US. Similar to optical imaging, PAI is depth limited; however, the power of the external light source can be adjusted to radiate sufficient energy into tissues 1–3 cm deep to generate sound. Similar to optical imaging, PAI also enables spectral specificity to recognize different absorbers such as oxy- and deoxy-hemoglobin. When MSCs are loaded with gold nanoparticles, an ideal PAI reporter, SCs can be detected *in vivo* [32].

Whereas PET, CT and MRI are quantitative, several uncontrolled variables related to the scanner, patient size and motion and attenuation make quantification with SPECT challenging. Similar limitations affect reporter quantification by US and PAI. Although US does not provide accurate absolute MB concentration, it does provide accurate relative difference in MB concentration between adjacent tissues within the same imaged field. Recently introduced sub-voxel resolution with MB suggests that an accurate MB count can potentially be provided over the entire field of view [33,34]. In addition to the same challenges as US, PAI also suffers from light attenuation that is different for each spectral wavelength.

Discussion of advantages and limitations of each specific imaging approach as they relate to SC imaging are presented below and in Table 1. Note that, with advances in computer and software capabilities, image fusion has become prevalent in the clinic. It enables the combination of PET – the highest sensitivity *in vivo* imaging tool – with the highest spatial resolution tool of CT or MRI. Fusion of real-time US imaging of patients that had been scanned with PET, CT or MRI, providing a 3D dataset, is currently used following either automatic co-registration or by use of fiducial markers. Although US fusion has not been used for molecular imaging, it is currently used in the clinic to biopsy lesions better seen on PET, CT or MRI under US guidance, which is more cost-effective and can be done at the bedside. Selected recent publications describing some aspects of SC labeling, imaging and tracking *in vivo* are shown in Table 2.

Advantages and challenges of SC imaging methods

Radionuclide imaging (PET and SPECT)

Nuclear imaging, particularly PET, has the highest *in vivo* sensitivity at a practical field of view, enabling a large array of labeling approaches to be deployed for SC applications in clinical practice. Further, the quantitative capabilities of PET, combined with its exceptional sensitivity, have made it the most popular imaging modality for SC tracking and assessment of cell viability [9,12–14,17]. Although PET and SPECT use radiotracers, the two technologies are significantly different [9,12–14,17]. There are several positron-emitting nuclei used in the clinic for PET imaging that vary in decay half-life from minutes (^{15}O and ^{13}N) to 1–2 h (^{18}F and ^{68}Ga) to nearly 13 h (^{64}Cu), with ^{18}F being the most commonly used tracer. The importance of half-life in direct SC labeling is that it limits the temporal window to label, administer and track cells as they home and accumulate in their target tissue. By contrast, SPECT radiotracers such as indium-111 (^{111}In) or metastable technicium-99m (^{99}mTc) emit gamma rays that are detected by a rotating gamma camera [35,36]. Compared with PET, SPECT has a lesser spatial resolution, and the lower gamma energy is more attenuated in the body; however, the half-life of its radiotracers: hours to days, is more favorable for SC labeling and tracking [17,36]. ^{111}In for instance has been used to label SCs for trafficking and biodistribution studies in large animal models [37,38]. Diverse tracers have been used for SC imaging with PET and SPECT, such as ^{18}FDG (fludeoxyglucose), ^{64}Cu-PTSM (pyruvaldehyde-bis(N^4-methylthiosemicarbazone)), ^{111}In-oxine and ^{99}mTc-HMPAO (hexamethylpropylene amine oxime) [12,14,17,39]. ^{18}FDG is the most commonly used PET tracer. It mimics glucose but is trapped intracellularly. Its rate of cellular uptake correlates with the cell's metabolic rate; however, for SC imaging it is used as a label before grafting [40]. Although it provides high sensitivity and low cytotoxicity, its half-life of 110 min makes it less suitable for longitudinal studies to monitor SC biodistribution and homing [12,41].

Because gamma-emitting radiotracers emit different energies, SPECT provides the option of dual-tracer imaging, for example ^{99}mTc (149.5 KeV) and ^{111}In (144 and 218 KeV) have been used to track different SC populations [42,43]. Whereas ^{111}In offers a longer monitoring window, ^{99}mTc can be given at higher doses because of its shorter half-life, to improve SNR for higher spatial resolution [14,36]. Several groups have directly labeled NSCs and MSCs with either ^{18}FDG [44,45] or ^{99}mTc-HMPAO [46]. There are several shortcomings to directly labeling SCs with radiotracers [13,14,17,37,42]. This approach is unable to recognize living from dead cells, is susceptible to tracer dilution because of cell division and migration, has a limited imaging window owing to relatively short decay times, delivers ionizing radiation potentially affecting SCs and, most importantly, imaging tracks the label not the SC [13,14,17,37,42]. To overcome the limited imaging time window, ^{52}Mn (5.5-day half-life) as well as ^{89}Zr (3.3-day half-life) were proposed, in addition to their longer half-lives, to have excellent stability and labeling efficiencies [36,47,48].

A better and more powerful approach is the use of reporter genes to detect gene expression to not only image SCs multiple times over a very long observation window but to also confirm cell viability [12,14,17]. There have been three different approaches. The best known and most widely used reporter genes for PET and SPECT imaging include the herpes simplex virus type 1 thymidine kinase (HSV1-tk) which is recognized as a hotspot where cells accumulate. HSV1-tk can be imaged with PET using ^{18}F-labeled acycloguanosine analog or fluoro-3-(hydroxymethyl)butylguanine ([^{18}F]FHBG). The second approach is to have the SC trap reporters in a region not known to accumulate the reporter, such as the sodium iodide symporter (NIS), a trans-membrane protein responsible for iodine transport in thyroid cells. SC accumulation is detected if SCs expressing NIS reside in tissues not known to trap iodine [9,13,16,49]. Similar to NIS, the third approach is when SCs express a receptor in tissues not known to have such a receptor. For example the expression of dopamine D_2 receptor (D2R) which is normally predominantly found in the *striata nigra*. D2R expression is imaged with PET following the administration of ^{18}F-labeled fallypride, a dopamine ligand [50]. Gene reporters enable SC imaging at any time and at multiple time points by administering the radiotracer to detect the expressed protein [14,16,51]. NIS imaging can also be done with ^{124}I for PET and ^{123}I for SPECT [51]. However, if not incorporated in the genome, the concentration of the expressed protein decreases over time with loss of the gene to natural decay and dilution because of cell division and migration.

MRI

MRI-based SC imaging provides high spatial resolution and reasonable imaging time (minutes) to noninvasively track labeled transplanted SCs [52,53]. MRI has been frequently used to monitor morphological and SC migration after engraftment [14,17]. MRI detects hydrogen atoms, the dominant atomic species in living systems. The signal is generated mostly from water and lipid hydrogens by detecting their resonant frequency which is unique to the location of a specific voxel within the field of view. Signal

TABLE 2

Selected recent publications describing some aspects of stem cell labeling, imaging and tracking *in vivo*

IImaging method	Cell type	Recipient species	Tracer or contrast agent(s)	Purpose	Refs
PET	Human mesenchymal stem cells	Mouse	^{89}Zr—desferrioxamine-NCS	PET-based noninvasive *in vivo* cell trafficking	Bansal *et al.*, 2015 [48]
PET	Autologous bone-marrow-derived stem cells (BMSCs)	Human	Fluorine 18-fluorodeoxyglucose (F-FDG)	To find administration methods for BMSCs in diabetic patients	Sood *et al.*, 2015 [40]
PET	hBMSCs	Mouse	Sodium iodide symporter (NIS) reporter gene	Hypoxia-based imaging and therapy strategy to target expression of the NIS gene to experimental hepatocellular carcinoma (HCC) delivered by MSCs	Muller *et al.*, 2016 [138]
PET-CT	Hematopoietic stem cells	Mouse	Fluorine 18-fluorodeoxyglucose (F-FDG)	To investigate hematopoietic stem cell homing efficacy	Faivre *et al.*, 2016 [41]
SPECT	Neural stem cells (NSC)	Mouse	$^{(111)}$ In conjugated mesoporous silica nanoparticles (MSN)	Noninvasive tracking of therapeutic NSCs toward glioblastoma	Cheng *et al.*, 2016 [139]
MRI	BMSC or NSC	Mouse	Superparamagnetic iron oxide nanoparticles (SPIO)	For tracking,SPIO labeled stem cells *in vivo* by MRI	Kim *et al.*, 2016 [57]
MRI	MSCs	Mouse	Gadolinium hybrid iron oxide (GdIO)	For dual T1- and T2-weighted MRI for cell labeling and tracking	Zeng *et al.*, 2017 [66]
MRI	Rat adipose derived stem cells (rASCs)	Rat	Caspase-3 sensitive nano-aggregation MRI probe (C-SNAM)	For noninvasive detection of stem cell apoptosis with MR imaging	Nejadnik *et al.*, 2015 [140]
US	Neural stem cells (NSC)	Mouse	Microbubbles	For ultrasound imaging *in vivo*	Cui *et al.*, 2013 [31]
US	Neural stem cells (NSC)	Mouse	Microbubbles	For ultrasound SC transfection *in vivo*	Tavri *et al.*,2013 [18]
US	Rat bone-marrow-derived MSCs	Mouse	Microbubbles	For the efficient transfection of MSCs	Haber *et al.*, 2017 [141]
US	Endogenous mesenchymal stem/ progenitor cells (MSCs)	Mini-pigs	Microbubbles	For *in situ* bone tissue engineering via ultrasound-mediated gene delivery	Bez *et al.*, 2017 [142]
Multimodal: BLI-MRI	Mouse glial precursor cells	Mouse	Luciferase gene −SPIO-NPs	To investigate the allograft survival within the brain	Janowski *et al.*, 2014 [105]
Multimodal: FLI-MRI	hMSCs	Mouse	Multimodal magnetic nanoclusters (M-MNCs)	For gene delivery, directed migration and tracking of SCs	Park *et al.*, 2017 [143]
Multimodal: FLI-CT	hMSCs	Mouse	Multifunctional stem cell nanotracer (M-NT)	For gene delivery and tracking stem cells	Park *et al.*, 2017 [144]
Multimodal:US-MRI	hMSCs	Mouse	Multimodal silica nanoparticles (SiNPs)	Real-time guided cell implantation using ultrasound, and high-resolution, long-term monitoring of SCs with MRI	Jokerst *et al.*, 2013 [87]
Multimodal: PET/MRI	hNPC	Rat	^{52}Mn; DMT1	Dual-modality PET/MR tracking of transplanted stem cells in the central nervous system	Lewis *et al.*, 2015 [114]
Multimodal: SPECT-CT	Rat fetal heart-MSC (fC-MSC)	Rat	99mTc HMPAO/PKH26 fluorescent dye	To evaluate cardiac perfusion, function and cell tracking after stem cell therapy in acute myocardial injury setting	Garikipati *et al.*, 2014 [115]

amplitude for each voxel is related to hydrogen concentration and their average magnetization within the voxel after perturbing them from equilibrium, which is dependent on their T1 and T2 relaxations. T2* effects result from magnetic inhomogeneity within the voxel. Observed effects of available contrast media are related to their concentration within the voxel and their influence on neighboring hydrogen T1 relaxation (T1 agents – increase signal) or their ability to induce magnetic inhomogeneity (T2* agents – decrease signal). Although there are pure T2 agents, their effects are weak. Nearly all successful MRI SC labeling strategies have been the result of preloading SCs with T1 or T2* agents, with the latter being most common [38]. Superparamagnetic iron oxide nanoparticles (SPIONs) 5–150 nm in size, depending on formulation, are the dominant T2* agents used, owing to their high relaxivity and excellent biocompatibility [19]. SPIONs can be easily incorporated within SCs in cell cultures that become visible *in vivo* as regions of signal loss [54], and have been shown to have no effect on SC viability, differentiation and therapeutic efficacy [55]. In early clinical studies, SPION labeling was used to track MSCs in patients with multiple sclerosis and amyotrophic lateral sclerosis [56], but have since expanded to track various SC types [4,57–59]. The size of iron oxide particles used has a marked effect on T2 shortening, where larger micron particles (MPIOs) have a several-fold greater effect than their smaller counterparts (SPIONs). Further, MPIOs improve labeling efficiency and particle retention. Their greater relaxivity has allowed the detection of smaller numbers of labeled SCs [60]. MPIO-labeled SCs have been used in cell-based therapies, regenerative medicine, as well as several types of human-derived normal and cancer SCs including glioma and glioblastoma [61]. The major limitations of iron-oxide-based labeling is their low uptake by SCs and more-important, particle dilution with cell proliferation and migration, decreasing detection [62]. Further, as with many reporter-labeled SCs, imaging tracks particles not SCs, leading to detection errors.

Chelated gadolinium-based reporters are the most widely used T1 agents. They increase MR signal easing target recognition so long as the target:background contrast:noise ratio is sufficient [14]. To achieve intracellular trapping, novel approaches of conjugating Gd in nanoparticles such as gold have been developed as efficient MRI contrast agents for molecular and cellular imaging [63–65]. In a recent study, biocompatible Gd hybrid iron oxide (GdIO) nanocomposites for dual T1- and T2*-weight imaging of stem cells were reported [66]. They demonstrated that the GdIO did not affect SC viability, proliferation or differentiation capacity [66]. However, these novel SC-labeling agents are too early in their development to truly assess their potential.

MR can image nuclei other than hydrogen, and ^{19}F has drawn most interest. ^{19}F is the most abundant form in nature and its resonance frequency is very close to that of the hydrogen that can be detected with properly tuned RF coils using most MR systems. ^{19}F resides in cancellous bone in living systems and is not detectable *in vivo*. Unfortunately, despite the absence of background signal, ^{19}F signal is low requiring much higher concentrations than hydrogen-based contrast agents for detection [67,68]. The highest concentration of exogenous ^{19}F is provided by PFCs that are typically composed of carbon and fluorine atoms that are immiscible in water and must be administered as emulsions [69,70]. These molecules are generally inert in living systems and are eliminated by exhalation with total body residence time ranging from minutes to years depending generally on their molecular weight. When cells are loaded with PFC emulsion particles, they can be tracked *in vivo*, and can be quantified [14,17,71,72]. Because these molecules are extremely inert, they have minor or no effect on cell viability, proliferation or differentiation [73]. Rose *et al.* labeled the stromal vascular fraction, which is a collection of cells, some of which are regenerative and are collected from liposuction material with CS-1000, a ^{19}F agent intended for a Phase I trial (clinicaltrials.gov identifier NCT02035085). They were able to detect 2×10^6 cells at 5 mm depth at 3-Tesla in a silicone phantom [74]. The major disadvantage of ^{19}F MRI is the relatively low signal and limited loading capacity of cells requiring 4×10^4 cells per voxel for detection [75], which could be improved by using stronger magnets, longer acquisition times or shortening ^{19}F T1 relaxation time [76]. Like all labeling with reporters, emulsion particles are also affected by dilution related to SC proliferation and migration.

There have been attempts at MR detection of gene expression, the ultimate labeling strategy for SC imaging *in vivo*. Unfortunately, the successes achieved with PET scanning have not been realized by MRI, mostly because of limited signal [12–14,17,77]. For instance, metalloproteins and metal ion transporters such as ferritin can be made to overexpress in transfected cells to enrich their intracellular content of iron and increase their detection on MRI [19,47,78]. A novel approach, described by Mukherjee *et al.*, uses aquaporin 1 (AQP1) which increases transmembrane water transport in transfected cells, and therefore water diffusion rates, increasing contrast on diffusion-weighted MRI [79]. The use of agents that enable chemical exchange saturation transfer (CEST) have become valuable tools for the detection of biomarkers such as temperature and pH [80,81], and have also been used to monitor the distribution of an extracellular hydrogel matrix after *in vivo* implantation [82].

MPI

MPI is a MR technique that requires different instrumentation to MRI. It uniquely detects superparamagnetic nanoparticles. Fortunately there is ample literature on labeling and tracking SCs with IONPs. MPI provides a more robust imaging technique to detect, localize and recognize IONPs with greater specificity than MRI. Because there is no background signal, high contrast images are produced, but require a 3D dataset such as that acquired with standard MRI or X-ray CT to anatomically localize detected signals. As with other direct labeling techniques, MPI images the reporter not the cell, and suffers from signal loss as cells divide and migrate.

Similar to protons, the magnetic moment of each IONP is randomly oriented with no resultant magnetic moment within a voxel. When a magnetic field gradient is applied, all particles become totally aligned with the magnetic field within a short distance from the zero-field – the point of inflection of the sigmoid shaped magnetization curve. The steeper the transition between the negative and positive magnetization curve the smaller the voxel size, which is also controlled by particle size and gradient strength. MPI takes advantage of this nonlinear behavior that is unique to superparamagnetic particles to limit detection to a small volume (~1 mm^3) that contains ~10 μM of IONPs with a 20 nm

particle size [28]. Detected signals are linear with concentration. Because signal is acquired one voxel at a time, which is raster scanned throughout the imaging volume, imaging time is dependent on the number of voxels acquired within the volume which ranges from milliseconds to several minutes depending on the voxel density desired. Faster imaging to achieve real-time scanning has been proposed [83]; however, these speeds continue to be at the expense of resolution and SNR.

MPI is extremely useful in SC tracking and assessing biodistribution over time in mice [27,84], and is quantitative with signal linearly tracking iron concentration regardless of aggregate geometry [29]. For instance, MPI showed that IONP-labeled MSCs injected systemically became trapped in the lungs, and subsequently migrated to the liver [84]. Using efficient cell labeling with IONPs and a prototype MPI system, 3–5 $\times$ 10^4 cells could be detected per voxel, which is similar to ^{19}F MRI with PFC labeling. The minimum number of cells that could theoretically be detected could be improved to <1000 cells per voxel with improved IONP formulation, instrumentation and cell labeling. MPI is dependent on IONP core size which defines signal and voxel size, with Resovist® producing a four-times greater signal than the older formulation Feridex®. Unfortunately, both of these clinical agents are no longer available creating yet another hurdle for translating MPI to the clinic. Several new formulations have been proposed specifically designed for MPI, which will require regulatory clearance before translation.

Ultrasound

Whereas several US contrast agents have been proposed over the years, PFC liquid droplets proposed in the early 1980s reached the clinic but required a minimum of 0.5 g (w/v)/kg dose to be visible on B-mode imaging [85]. Although SCs loaded with PFC are detectable by ^{19}F MRI, the amount of liquid PFC loaded and the number of cells used for MR detection are insufficient for standard US detection. However, should SCs be loaded with PFC vapor as 1–2 μm MB, a single cell can be detected *in vivo* (Fig. 2) [31]. This exquisite sensitivity to MB is due to the PFC vapor that stabilizes them and the unique frequencies emitted when MB oscillate in the US field. Further, when MBs are intracellular they not only survive for days rather than minutes when they are free in plasma, but they also become less sensitive to destruction when exposed to US [31]. US-based SC imaging is not only the most sensitive of the available *in vivo* imaging techniques but US can also track MB-labeled SCs for days [31,86,87]. US tracking of SCs has been reported using SC labeling with MB, acoustically active liposomes and theranostic mesoporous silica nanoparticles [88,89]. As an alternative to directly labeling SCs, Kuliszewski *et al.* used gene expression to detect SCs [90]. Engrafted endothelial progenitor cells (EPCs) were made to express a unique surface receptor that was used as a target for MB carrying the specific ligand to detect the implanted SCs [90]. With this approach, SCs must be exposed to blood to be able to interact with MB, because the 1–3 μm MB size limits them to the intravascular space. Should US agents be made nanoscale and targeted, gene expression that expresses surface receptors can be used to detect SCs *in vivo* and confirm viability. Once SCs are loaded with MB, they experience the same radiation force experienced by free MB forcing them against the deeper vascular wall to enhance targeting, adhesion and potentially migration [91,92]. In fact, MB labeling for SC detection need not be intracellular, rather, MB can be targeted to and attached to surface receptors [91,92].

The lipid shell of MB used for SC labeling can also be loaded with DNA, which upon exposure to US can effectively deliver genes to transfect the labeled SCs (Fig. 2) [18]. Should the pressure required for transfection be greater than that required for detection, it would be possible to monitor SC accumulation at the site of interest, and then transfect SCs at the desired time and space to induce the desired function, as was shown feasible *in vitro* [31] and *in vivo* [18]. Recent developments in high-intensity-focused US have enhanced the efficacy of SC therapy [93]. Despite these advances and the high sensitivity of US, US reporters loaded within SCs before engraftment suffer the same drawback of dilution with cell division and migration. However, we suspect that, upon cell death, MB will become free and short lived eliminating the label from the imaging field, suggesting that visible signal is indicative of viable cells.

Inspired by gas-vesicle-forming photosynthetic microbes, which produce these vesicles to control the organisms' buoyancy, Shapiro *et al.* characterized these gas vesicles that also contain iron and showed that they are active as US and MRI contrast agents [94–96]. The genetic precursors of these complex protein vesicles were then determined and used as a US and MRI gene reporter system [96]. The extremely high sensitivity of US should prove to be a powerful tool to label and track SCs.

PAI

Several PAI contrast agents have been proposed focusing on unique absorbers. A novel PFC emulsion-based PAI agent incorporates gold nanoparticles within the PFC phase. Not only do these emulsions absorb transmitted light but the localized heating evaporates the surrounding PFC liquid to generate nanobubbles increasing US signal [32]. Prussian blue nanoparticles have also been proposed as PAI agents with strong optical absorption in the near-infrared region [97]. Their optical properties allow the use of 730 nm lasers, improving light penetration, with adequate sensitivity as determined by subcutaneous injections (theoretical limit of 200 cells/mm^3). Further, the administration of 5 $\times$ 10^4 MSCs could be followed in mice for 14 days [97]. Similar results were reported using hESC-CMs in living mouse hearts labeled with semiconducting polymers that also absorb in the 700 nm range [98]. With this label, they also showed the detection limit to be 200 cells/mm^3 following subcutaneous injection.

Optical imaging

Fluorescence and bioluminescence are the two major optical imaging methods that are widely used for preclinical experiments to assess location and functional status of SCs [17,79]. FLI transmits light into tissues to excite fluorophores and receives the emitted fluorescence. It provides excellent sensitivity and is able to image and track SCs at the cellular level [14,42]. Classically, cells are labeled with fluorescent dyes or engineered to express a fluorescent protein preferably in the near-infrared range to enable greater imaging depth for *in vivo* detection [99]; however, FLI is practical in only mice or superficial structures owing to severe light scattering and absorption, as well as limited emission per molecule and photobleaching, limiting translation [12,14,36,99]. To maximize reporter labeling, fluorescent polymeric NPs and quantum dots (QDs) have been used

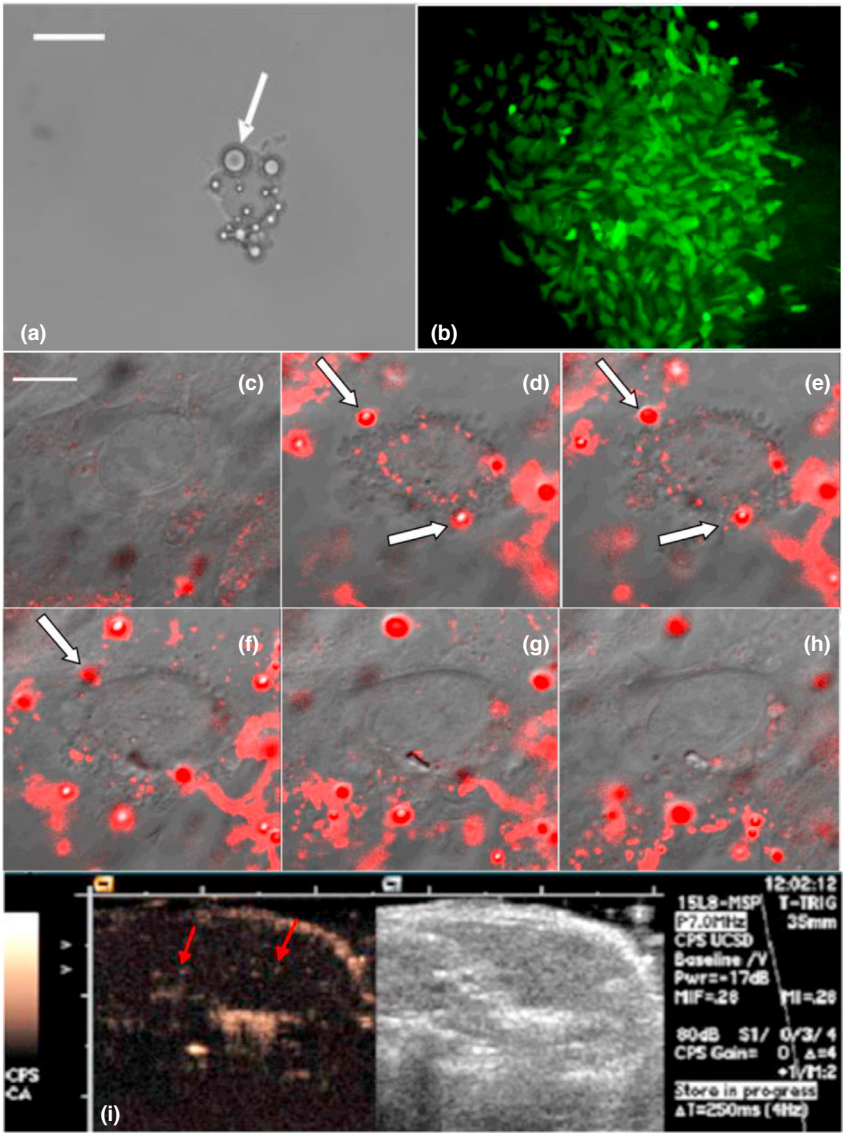

FIGURE 2

This figure was adapted, with permission, from [31]. **(a)** Single trypsinized neuroprogenitor cell (NPC) containing multiple microbubbles (MB) (arrows) appearing as black circles with a white center owing to light diffraction (scale bar = 10 μm). **(b)** NPC culture acquired 48 h following ultrasound exposure of GFP-carrying MB loaded within NPC. **(c–h)** Confocal microscopy of DiI-labeled MB showing the time course of internalization of several MB by NPCs (arrow) that disappear as they move out of the 0.8 μm slice (scale bar = 10 μm). **(i)** MB-only and its corresponding B-mode images of a mouse liver acquired with a 2.4 cm depth of field, 5 days after the i.v. administration of 1.5×10^6 MB-labeled NPCs shortly following 20 mg sodium nitroprusside given i.v. to minimize NPC lung trapping. Note that at 5 days several MB-labeled NPCs are still visible (red arrows). Scale bars in a and c–h = 10 μm.

to label and monitor SCs [15], as well as monitor their accumulation in wound healing using a chemoattractants [100]. An interesting method of cell labeling is the direct introduction of reporter into the cytoplasm using sonoporation with US and MB, or photoporation with light and gold nanoparticles [101]. Using photoporation, Xiong *et al.* showed a several-fold increase in labeling efficiency, symmetric signal distributed to daughter cells and the reporter remained visible for 2 months rather than 2 weeks [101].

Although novel FLI techniques have been proposed to improve signal recognition from tissue autofluorescence using fluorescence lifetime imaging, imaging deeper than a few millimeters *in vivo* with acceptable resolution remains a significant challenge. Fortunately, however, the majority of studies showed that FLI reporters did not affect SC viability or function, but the highest concentration of QDs caused cytotoxicity [15].

Bioluminescence imaging (BLI) detects light generated in tissues. The typical source of light is when luciferase catalyzes its substrate luciferin. Cells are typically engineered to express luciferase, and luciferin is typically given intraperitoneally for imaging [12,14,17,36]. Because catalysis can only occur in living cells, BLI can track SCs expressing luciferase as well as assess SC viability. Luciferase can be of firefly or *Renilla* origin, which catalyze luciferin or coelenterazine, respectively. Because emitted photons have different wavelengths, both systems can be used simultaneously to track different SC populations [102]. BLI has been extensively used for tracking SCs *in vivo*, including ESCs and NSCs in small animals

[16,103–105] and, when the luciferase gene is stably transfected, cells can be imaged over a long period after engraftment by merely administering the substrate [102,103]. Note that photon generation is ATP-dependent [103], requires oxygen [106] and the substrate must reach the SCs of interest in concentrations sufficient to generate enough photons for detection within a reasonable acquisition time. Substrate delivery is affected by administration route, blood flow, serum protein binding capacity, the inhibitory effect of volatile anesthetics and the general physiological state of the animal [107,108]. Because emitted photons are also scattered and attenuated by tissues, the number of photons reaching the detector limits detection to a shallow depth or requires a longer integration time. A recent exciting opportunity is the introduction of a totally synthetic enzyme that catalyzes a synthetic luciferin-like substrate that has superior biodistribution to luciferin. More important is that gene expression is fourfold more efficient, catalysis is sevenfold more effective and the emitted photon is red-shifted at 650 nm (several orders brighter) and can reach the detector from deeper regions allowing the detection of a few labeled cells and the ability to detect labeled cells *in vivo* in real-time [109].

Multimodal imaging

With the advent of rapid computing and the ability to fuse images acquired by different imaging modalities either concurrently or in different imaging sessions, it has become possible to combine the advantages of different imaging techniques [87,110]. The most developed and clinically used is PET-CT which combines the high spatial resolution of CT with the high reporter sensitivity of PET [13]. PET-MR is becoming more available, taking advantage of the added capabilities afforded by MRI. In addition to spatially combining imaging data, information gleaned from one technique can be used to improve image quality of the other, such as adjusting for tissue attenuation in PET imaging based on X-ray attenuation defined by CT [111]. These added capabilities have brought a new perspective to SC imaging. Multimodal imaging has allowed the use of different tracers for multiparametric imaging [73,112]. Thus, a combination of PET or SPECT with MRI can provide superior resolution, higher tracer sensitivities, as well as greater functionality [113]. Combinations of MRI with PET [114], BLI with MRI and SPECT with FLI have been reported [115]. For instance, the combination of MRI and BLI was successfully used to assess SC fate *in vivo*, enabling functional evaluation in myocardial infarction [116].

Key challenges in clinical translation

Noninvasive SC imaging and monitoring can provide a comprehensive assessment of SC therapy. Even though successes have been achieved in preclinical models, translation to the clinic has met with several challenges. In addition to the fact that SC imaging strategies and efficiencies have numerous advantages when developed in rodents, differences in physiology, pharmacokinetics, basal metabolic rates, among others, are considerable, limiting prediction of clinical success [117]. Transitioning to larger animal models and those with more-appropriate physiology to humans could bridge the translational gap.

SC survival, biodistribution and differentiation

Success of SC therapy in the clinic has been unpredictable, probably owing to inconsistent SC survival, varied biodistribution with entrapment in the liver, spleen, lung and bone marrow in case of systemic administration, and success of engraftment if directly delivered to the site of interest, and ultimately SC differentiation into the desired function sought. For instance, it was shown that <10% of administered SCs were engrafted in the tissue of interest – the remainder became trapped in the reticuloendothelial organs or died shortly after implantation [118,119]. Imaging provides the opportunity to ensure that SCs are engrafted in the tissue of interest, are alive and ultimately differentiated into the desired function. Unfortunately, as the number of SCs and reporter concentration decreases, it becomes more challenging for imaging to detect and assess the engrafted SCs [14]. Tracking SCs to confirm they reached the tissue of interest is the easiest problem to navigate because loading SCs with reporters can be optimized to achieve the desired sensitivity and spatial resolution for the imaging modality used. Further, in the case of radioisotopes, the appropriate decay half-life has to be long enough to provide a sufficient imaging time window to track the SCs. Although indirect labeling with reporter genes infers SC viability and is the preferred technique, their detection *in vivo* is more challenging than direct labeling, mostly because of limited reporter concentration which is dependent on robust gene expression and the presence of a sufficient number of SCs at the site of interest. Further, stably transfected engineered cells raise safety concerns.

Safety concerns

Clinical implementation of SC-based therapy has been hindered by the potential for tumorigenesis. SCs have natural tropism to cancer and can be induced by the tumor to promote growth. Unfortunately, SCs also have the potential to form tumors themselves, particularly when ESCs or iPSCs are used. Successful monitoring of delivered SCs could allow the detection of early tumor formation. Although short-term monitoring of SCs *in vivo* has been achieved in clinical trials using radionuclide-based methods, long-term monitoring is still problematic and no clinically acceptable technique has emerged.

Complex regulatory requirement

The inclusion of SC imaging in clinical trials adds complexity to the regulatory process requiring details of the labeling methods, labeling efficiency and label concentration, as well as the effect of labeling on SC viability, proliferation, migration, function and tumorigenicity. It is therefore imperative that labeling does not impact SC potency, interfere with their function or introduce a new undesired effect. These safety requirements increase further when SCs are engineered to express a reporter gene. In addition to validating gene expression, stability and long-term passaging and lack of tumorigenesis need to be confirmed [12,13]. If multiple genes are incorporated, for example the addition of a suicide gene, expression of the genes and the programed functions need to be confirmed, for example cell death when the suicide gene is triggered [13]. In addition, SC dose, administration schedule, route of administration, intended sites and target organ accumulation need to be defined [120]. Using nonclinically approved products during the manufacturing process should be avoided to ease translation, such as the use of fetal bovine serum or dimethylsulfoxide.

Concluding remarks and future directions

Given the limitations of spatial resolution, reporter sensitivity, depth of field or labeling strategies of existing imaging methods, advances in image fusion enabling multimodal imaging holds great promise in supporting SC imaging in clinical trials. In addition to combining imaging advantages of each of the two fused modalities, different reporter systems detectable by each of these imaging techniques enables strategies that can improve tracking, recognize engraftment and confirm functional differentiation. Novel labeling strategies that can increase short-term monitoring time to enable SC tracking for 1–2 days to ensure that they reach their intended destination, and strategies that enable long-term monitoring to assess migration, proliferation, function and survival, while not affecting SC function or inducing malignant degeneration, are needed. In addition, including the possibility of interacting with engrafted SCs using US or light to induce a desired functional change with spatial and temporal specificity would be of great benefit for specific applications, particularly if the desired change initiates a therapeutic effect or activates a SC suicidal pathway.

SCs have generally been administered intravenously to mimic endogenous physiological SC delivery. However, because a large fraction becomes trapped in the lungs because of surface adhesion molecules [121,122] or as aggregates, intra-arterial delivery might be more effective at increasing SC concentration in target organs [122]. Ineffective or temporarily effective SC therapy could in part be due to suboptimal SC delivery [123]. Strategies to more effectively deliver SCs to tissues and organs have been proposed aiming to enhance therapeutic efficacy at a reduced SC dose [124–126]. Such approaches, for example image-guided SC delivery, have been used in the heart [127], brain [128], spinal cord [129], liver [130] and kidney [131]. However, local injections or implantation could disrupt native tissue architecture and create several adverse effects [132]. It should be noted that, assuming successful delivery and engraftment, SCs are potentially susceptible to the pathological environment of the host tissue, accelerating SC death or decreasing potency [133]. Advances in SC genetic modifications, such as site-specific integration using phage integrases [134], transcription activator-like effector nuclease (TALEN) [135] or clustered regularly interspaced short palindromic repeats (CRISPR) [136], hold great promise. 3D printed tissues have shown remarkable regenerative capabilities and the progress of 3D printed tissues has been reviewed by Choi *et al.* [137]. In their review, the authors express the need to monitor the viability of the fabricated scaffolds and the performance of printed tissues *in vitro and in vivo* to help advance the field. Our review focuses on SC imaging to support SC therapy; however, imaging should also be incorporated in trials to monitor ultimate therapeutic efficacy and safety to better asses the risk:benefit ratio.

Acknowledgments

R.F.M. is an Established Investigator Scholar of the Cancer Prevention Research Institute of Texas (CPRIT); R.F.M. and R.J.C.B. received salary support from CPRIT grant RR150010.

Conflicts of interest

The authors state that they have no conflicts of interest to declare.

References

1 Mason, C. *et al.* (2011) Cell therapy industry: billion dollar global business with unlimited potential. *Regen. Med.* 6, 265–272
2 Trounson, A. and DeWitt, N.D. (2016) Pluripotent stem cells progressing to the clinic. *Nat. Rev. Mol. Cell Biol.* 17, 194–200
3 Boregowda, S.V. *et al.* (2016) A clinical indications prediction scale based on TWIST1 for human mesenchymal stem cells. *EBioMed* 4, 62–73
4 Egawa, E.Y. *et al.* (2015) A DNA hybridization system for labeling of neural stem cells with SPIO nanoparticles for MRI monitoring post-transplantation. *Biomaterials* 54, 158–167
5 Wainger, B.J. *et al.* (2014) Intrinsic membrane hyperexcitability of amyotrophic lateral sclerosis patient-derived motor neurons. *Cell Rep.* 7, 1–11
6 Mandai, M. *et al.* (2017) Autologous induced stem-cell–derived retinal cells for macular degeneration. *N. Eng. J. Med.* 376, 1038–1046
7 Barker, R.A. *et al.* (2016) Are stem cell-based therapies for Parkinson's disease ready for the clinic in 2016? *J. Parkinson's Dis.* 6, 57–63
8 Raju, R. *et al.* (2017) Cell expansion during directed differentiation of stem cells toward the hepatic lineage. *Stem Cells Dev* 26, 274–284
9 Trounson, A. and McDonald, C. (2015) Stem cell therapies in clinical trials: progress and challenges. *Cell Stem Cell* 17, 11–22
10 Kovacic, J.C. and Fuster, V. (2015) *Cell Therapy For Patients With Acute Myocardial Infarction.* American Heart Association
11 Stuckey, D.W. and Shah, K. (2014) Stem cell-based therapies for cancer treatment: separating hope from hype. *Nat. Rev. Cancer* 14, 683–691
12 Nguyen, P.K. *et al.* (2014) Stem cell imaging: from bench to bedside. *Cell Stem Cell* 14, 431–444
13 Naumova, A.V. *et al.* (2014) Clinical imaging in regenerative medicine. *Nat. Biotechnol.* 32, 804–818
14 Gu, E. *et al.* (2012) Molecular imaging of stem cells: tracking survival, biodistribution, tumorigenicity, and immunogenicity. *Theranostics* 2, 335–345
15 Wang, Y. *et al.* (2013) Commercial nanoparticles for stem cell labeling and tracking. *Theranostics* 3, 544–560
16 Wang, J. and Jokerst, J.V. (2016) Stem cell imaging: tools to improve cell delivery and viability. *Stem Cells Int.* 2016, 9240652
17 Gavins, F.N. and Smith, H.K. (2015) Cell tracking technologies for acute ischemic brain injury. *J. Cereb. Blood Flow Metab.* 35, 1090–1099
18 Tavri, S. *et al.* (2015) *In vivo* transfection and detection of gene expression of stem cells preloaded with DNA-carrying microbubbles. *Radiology* 276, 518–525
19 Naumova, A.V. *et al.* (2010) Ferritin overexpression for noninvasive magnetic resonance imaging-based tracking of stem cells transplanted into the heart. *Mol. Imaging* 9, 201–210
20 Toyokuni, T. *et al.* (1999) Repetitive, non-invasive imaging of the dopamine D2 receptor as a reporter gene in living animals. *Gene Ther.* 6, 785–791
21 Green, L.A. *et al.* (2004) A tracer kinetic model for 18F-FHBG for quantitating herpes simplex virus type 1 thymidine kinase reporter gene expression in living animals using PET. *J. Nucl. Med.* 45, 1560–1570
22 Huang, N.F. *et al.* (2012) Bioluminescence imaging of stem cell-based therapeutics for vascular regeneration. *Differentiation* 41, 42
23 Girard, O.M. *et al.* (2011) Optimization of iron oxide nanoparticle detection using ultrashort echo time pulse sequences: comparison of T1, T2*, and synergistic T1–T2* contrast mechanisms. *Magn. Reson. Med.* 65, 1649–1660
24 Heyn, C. *et al.* (2006) *In vivo* magnetic resonance imaging of single cells in mouse brain with optical validation. *Magn. Res. Med.* 55, 23–29
25 Gleich, B. and Weizenecker, J. (2005) Tomographic imaging using the nonlinear response of magnetic particles. *Nature* 435, 1214–1217
26 Lu, K. *et al.* (2017) Multi-channel acquisition for isotropic resolution in magnetic particle imaging. *IEEE Trans. Med. Imaging* 37, 1989–1998
27 Zheng, B. *et al.* (2015) Magnetic particle imaging tracks the long-term fate of *in vivo* neural cell implants with high image contrast. *Sci. Rep.* 5, 14055
28 Weizenecker, J. *et al.* (2007) A simulation study on the resolution and sensitivity of magnetic particle imaging. *Phys. Med. Biol.* 52, 6363–6374
29 Bulte, J.W. *et al.* (2015) Quantitative "hot spot" imaging of transplanted stem cells using superparamagnetic tracers and magnetic particle imaging (MPI). *Tomography* 1, 91–97
30 Klibanov, A.L. *et al.* (2004) Detection of individual microbubbles of ultrasound contrast agents: imaging of free-floating and targeted bubbles. *Invest. Radiol.* 39, 187–195

31 Cui, W. *et al.* (2013) Neural progenitor cells labeling with microbubble contrast agent for ultrasound imaging *in vivo*. *Biomaterials* 34, 4926–4935
32 Nam, S.Y. *et al.* (2012) *In vivo* ultrasound and photoacoustic monitoring of mesenchymal stem cells labeled with gold nanotracers. *PLoS One* 7, e37267
33 Ghosh, D. *et al.* (2017) Toward optimization of *in vivo* super-resolution ultrasound imaging using size-selected microbubble contrast agents. *Med. Phys.* 44, 6304–6313
34 Tanigaki, K. *et al.* (2018) Hyposialylated IgG activates endothelial IgG receptor FcgammaRIIB to promote obesity-induced insulin resistance. *J. Clin. Invest.* 128, 309–322
35 Chan, A.T. and Abraham, M.R. (2012) Ffrom bench to imaging SPECT and PET to optimize cardiac stem cell therapy. *J. Nucl. Cardiol.* 19, 118–125
36 Von der Haar, K. *et al.* (2015) Lost signature: progress and failures in *in vivo* tracking of implanted stem cells. *Appl. Microbiol. Biotechnol.* 99, 9907–9922
37 Leibacher, J. and Henschler, R. (2016) Biodistribution, migration and homing of systemically applied mesenchymal stem/stromal cells. *Stem Cell Res. Ther.* 7, 7
38 Cen, P. *et al.* (2016) Noninvasive in-vivo tracing and imaging of transplanted stem cells for liver regeneration. *Stem Cell Res. Ther.* 7, 143
39 Legacz, M. *et al.* (2014) Contrast agents and cell labeling strategies for *in vivo* imaging. *Adv. Nanoparticles* 3, 41–53
40 Sood, V. *et al.* (2015) Biodistribution of 18F-FDG-labeled autologous bone marrow-derived stem cells in patients with type 2 diabetes mellitus: exploring targeted and intravenous routes of delivery. *Clin. Nucl. Med.* 40, 697–700
41 Faivre, L. *et al.* (2016) 18 F-FDG labelling of hematopoietic stem cells: dynamic study of bone marrow homing by PET–CT imaging and impact on cell functionality. *Curr. Res. Transl. Med.* 64, 141–148
42 Kircher, M.F. *et al.* (2011) Noninvasive cell-tracking methods. *Nat. Rev. Clin. Oncol.* 8, 677–688
43 Guo, Z. *et al.* (2016) Simultaneous SPECT imaging of multi-targets to assist in identifying hepatic lesions. *Sci. Rep.* 6, 28812
44 Stojanov, K. *et al.* (2012) 18F FDG labeling of neural stem cells for *in vivo* cell tracking with positron emission tomography: inhibition of tracer release by phloretin. *Mol. Imaging* 11 7290.2011. 00021
45 Wolfs, E. *et al.* (2013) 18F-FDG labeling of mesenchymal stem cells and multipotent adult progenitor cells for PET imaging: effects on ultrastructure and differentiation capacity. *J. Nucl. Med.* 54, 447–454
46 Verma, V. *et al.* (2014) *In vitro* assessment of cytotoxicity and labeling efficiency of 99m Tc-HMPAO with stromal vascular fraction of adipose tissue. *Nucl. Med. Biol.* 41, 744–748
47 Bartelle, B.B. *et al.* (2013) Divalent metal transporter, DMT1: A novel MRI reporter protein. *Magn. Res. Med.* 70, 842–850
48 Bansal, A. *et al.* (2015) Novel 89 Zr cell labeling approach for PET-based cell trafficking studies. *EJNMMI Res.* 5, 19
49 Holvoet, B. *et al.* (2015) Sodium iodide symporter PET and BLI noninvasively reveal mesoangioblast survival in dystrophic mice. *Stem Cell Rep.* 5, 1183–1195
50 Haralampieva, D. *et al.* (2016) Noninvasive PET imaging and tracking of engineered human muscle precursor cells for skeletal muscle tissue engineering. *J. Nucl. Med.* 57, 1467–1473
51 Penheiter, A.R. *et al.* (2012) The sodium iodide symporter (NIS) as an imaging reporter for gene, viral, and cell-based therapies. *Curr. Gene Ther.* 12, 33–47
52 Liu, L. *et al.* (2016) A new method for preparing mesenchymal stem cells and labeling with ferumoxytol for cell tracking by MRI. *Sci. Rep.* 6, 26271
53 Goodfellow, F.T. *et al.* (2016) Tracking and quantification of magnetically labeled stem cells using magnetic resonance imaging. *Adv. Funct. Mater.* 26, 3899–3915
54 Li, L. *et al.* (2013) Superparamagnetic iron oxide nanoparticles as MRI contrast agents for non-invasive stem cell labeling and tracking. *Theranostics* 3, 595–615
55 Yang, Y. *et al.* (2013) Superparamagnetic iron oxide is suitable to label tendon stem cells and track them *in vivo* with MR imaging. *Annal. Biomed. Eng.* 41, 2109–2119
56 Karussis, D. *et al.* (2010) Safety and immunological effects of mesenchymal stem cell transplantation in patients with multiple sclerosis and amyotrophic lateral sclerosis. *Arch. Neurol.* 67, 1187–1194
57 Kim, S.J. *et al.* (2016) Superparamagnetic iron oxide nanoparticles for direct labeling of stem cells and *in vivo* MRI tracking. *Contrast Media Mol. Imaging* 11, 55–64
58 Daldrup-Link, H.E. *et al.* (2017) Detection of stem cell transplant rejection with ferumoxytol MR imaging: correlation of MR imaging findings with those at intravital microscopy. *Radiology* http://dx.doi.org/10.1148/radiol.2017161139
59 Skelton, R. *et al.* (2016) Magnetic resonance imaging of iron oxide-labeled human embryonic stem cell-derived cardiac progenitors. *Stem Cells Transl. Med.* 5, 67–74
60 Shapiro, E.M. *et al.* (2006) *In vivo* detection of single cells by MRI. *Magn. Res. Med.* 55, 242–249
61 Boulland, J.-L. *et al.* (2012) Evaluation of intracellular labeling with micron-sized particles of iron oxide (MPIOs) as a general tool for *in vitro* and *in vivo* tracking of human stem and progenitor cells. *Cell Transplant.* 21, 1743–1759
62 Xu, C. *et al.* (2012) Tracking mesenchymal stem cells with iron oxide nanoparticle loaded poly (lactide-co-glycolide) microparticles. *Nano Lett.* 12, 4131–4139
63 Faucher, L. *et al.* (2012) Rapid synthesis of PEGylated ultrasmall gadolinium oxide nanoparticles for cell labeling and tracking with MRI. *ACS Appl. Mater. Interface* 4, 4506–4515
64 Rammohan, N. *et al.* (2016) Gd(III)-Gold nanoconjugates provide remarkable cell labeling for high field magnetic resonance imaging. *Bioconj. Chem.* 28, 153–160
65 Randolph, L.M. *et al.* (2016) Polymeric Gd-DOTA amphiphiles form spherical and fibril-shaped nanoparticle MRI contrast agents. *Chem. Sci.* 7, 4230–4236
66 Zeng, Y. *et al.* (2017) Gadolinium hybrid iron oxide nanocomposites for dual T 1- and T 2-weighted MR imaging of cell labeling. *Biomater. Sci.* 5, 50–56
67 Srinivas, M. *et al.* (2010) 19 F MRI for quantitative *in vivo* cell tracking. *Trends Biotechnol.* 28, 363–370
68 Gaudet, J.M. *et al.* (2016) Application of dual 19F and iron cellular MRI agents to track the infiltration of immune cells to the site of a rejected stem cell transplant. *Magn. Res. Med.* 78, 713–720
69 Mattrey, R.F. (1989) Perfluorooctylbromide: a new contrast agent for CT, sonography, and MR imaging. *Am. J. Roentgenol.* 152, 247–252
70 Riess, J.G. (1984) Reassessment of criteria for the selection of perfluorochemicals for second-generation blood substitutes: analysis of structure/property relationships. *Artif. Organs* 8, 44–56
71 Vu-Quang, H. *et al.* (2016) Chitosan-coated poly (lactic-co-glycolic acid) perfluorooctyl bromide nanoparticles for cell labeling in 19 F magnetic resonance imaging. *Carbohydr. Polym.* 136, 936–944
72 Gaudet, J.M. *et al.* (2015) Tracking the fate of stem cell implants with fluorine-19 MRI. *PloS One* 10, e0118544
73 Boehm-Sturm, P. *et al.* (2014) A multi-modality platform to image stem cell graft survival in the naïve and stroke-damaged mouse brain. *Biomaterials* 35, 2218–2226
74 Rose, L.C. *et al.* (2015) Fluorine-19 labeling of stromal vascular fraction cells for clinical imaging applications. *Stem Cells Transl. Med.* 4, 1472–1481
75 Ruiz-Cabello, J. *et al.* (2008) *In vivo* "hot spot" MR imaging of neural stem cells using fluorinated nanoparticles. *Magn. Reson. Med.* 60, 1506–1511
76 Kislukhin, A.A. *et al.* (2016) Paramagnetic fluorinated nanoemulsions for sensitive cellular fluorine-19 magnetic resonance imaging. *Nat. Mater.* 15, 662–668
77 Lee, S.-W. *et al.* (2012) Magnetic resonance reporter gene imaging. *Theranostics* 2, 403–412
78 Patrick, P.S. *et al.* (2014) Dual-modality gene reporter for *in vivo* imaging. *Proc. Natl. Acad. Sci.* 111, 415–420
79 Mukherjee, A. *et al.* (2016) Non-invasive imaging using reporter genes altering cellular water permeability. *Nat. Commun.* 7, 13891
80 Chan, K.W. *et al.* (2013) MRI-detectable pH nanosensors incorporated into hydrogels for *in vivo* sensing of transplanted-cell viability. *Nat. Mater.* 12, 268–275
81 Ziv, K. and Gambhir, S.S. (2013) Bioengineering and regenerative medicine: keeping track. *Nat. Mater.* 12, 180–181
82 Jin, T. *et al.* (2017) Diamagnetic chemical exchange saturation transfer (diaCEST) affords magnetic resonance imaging of extracellular matrix hydrogel implantation in a rat model of stroke. *Biomaterials* 113, 176–190
83 Weizenecker, J. *et al.* (2009) Three-dimensional real-time *in vivo* magnetic particle imaging. *Phys. Med. Biol.* 54, L1–10
84 Zheng, B. *et al.* (2016) Quantitative magnetic particle imaging monitors the transplantation, biodistribution, and clearance of stem cells *in vivo*. *Theranostics* 6, 291–301
85 Behan, M. *et al.* (1993) Perfluorooctylbromide as a contrast agent for CT and sonography: preliminary clinical results. *Am. J. Roentgenol.* 160, 399–405
86 Hartanto, J. and Jokerst, J.V. (2017) Nanoparticles for ultrasound-guided imaging of cell implantation. In *Design and Applications of Nanoparticles in Biomedical Imaging* (Bulte, J.W.M. and Modo, M.M.J., eds), pp. 299–314, Springer
87 Jokerst, J.V. *et al.* (2013) Intracellular aggregation of multimodal silica nanoparticles for ultrasound-guided stem cell implantation. *Sci. Transl. Med.* 5 177ra35–177ra35
88 Kempen, P.J. *et al.* (2015) Theranostic mesoporous silica nanoparticles biodegrade after pro-survival drug delivery and ultrasound/magnetic resonance imaging of stem cells. *Theranostics* 5, 631
89 Herbst, S.M. *et al.* (2009) Delivery of stem cells to porcine arterial wall with echogenic liposomes conjugated to antibodies against CD34 and intercellular adhesion molecule-1. *Mol. Pharm.* 7, 3–11
90 Kuliszewski, M.A. *et al.* (2009) Molecular imaging of endothelial progenitor cell engraftment using contrast-enhanced ultrasound and targeted microbubbles. *Cardiovasc. Res.* 83, 653–662
91 Kaya, M. *et al.* (2012) Acoustic radiation force for vascular cell therapy: *in vitro* validation. *Ultrasound Med. Biol.* 38, 1989–1997
92 Toma, C. *et al.* (2011) Vascular endoluminal delivery of mesenchymal stem cells using acoustic radiation force. *Tissue Eng. A* 17, 1457–1464

93 Wang, G. *et al.* (2016) Effects of diagnostic ultrasound-targeted microbubble destruction on the homing ability of bone marrow stromal cells to the kidney parenchyma. *Eur. Radiol.* 26, 3006–3016
94 Shapiro, M.G. *et al.* (2014) Biogenic gas nanostructures as ultrasonic molecular reporters. *Nat. Nanotechnol.* 9, 311–316
95 Maresca, D. *et al.* (2017) Nonlinear ultrasound imaging of nanoscale acoustic biomolecules. *Appl. Phys. Lett.* 110, 073704
96 Lu, G.J. *et al.* (2018) Proteins, air and water: reporter genes for ultrasound and magnetic resonance imaging. *Curr. Opin. Chem. Biol.* 45, 57–63
97 Kim, T. *et al.* (2017) Photoacoustic imaging of human mesenchymal stem cells labeled with Prussian blue-poly(L-lysine) nanocomplexes. *ACS Nano* 11, 9022–9032
98 Qin, X. *et al.* (2018) Photoacoustic imaging of embryonic stem cell-derived cardiomyocytes in living hearts with ultrasensitive semiconducting polymer nanoparticles. *Adv. Funct. Mater.* 28, 1704939
99 Hoffman, R.M. (2005) The multiple uses of fluorescent proteins to visualize cancer *in vivo*. *Nat. Rev. Cancer* 5, 796–806
100 Chen, G. *et al.* (2015) *In vivo* real-time visualization of mesenchymal stem cells tropism for cutaneous regeneration using NIR-II fluorescence imaging. *Biomaterials* 53, 265–273
101 Xiong, R. *et al.* (2016) Cytosolic delivery of nanolabels prevents their asymmetric inheritance and enables extended quantitative *in vivo* cell imaging. *Nano Lett.* 16, 5975–5986
102 Kang, J.H. and Chung, J.-K. (2008) Molecular-genetic imaging based on reporter gene expression. *J. Nucl. Med.* 49, 164S–179S
103 Peeters, M. *et al.* (2015) Bioluminescence-mediated longitudinal monitoring of adipose-derived stem cells in a large mammal *ex vivo* organ culture. *Sci. Rep.* 5, 13960
104 Allen, A.B. *et al.* (2014) *In vivo* bioluminescent tracking of mesenchymal stem cells within large hydrogel constructs. *Tissue Eng. C: Methods* 20, 806–816
105 Janowski, M. *et al.* (2014) Survival of neural progenitors allografted into the CNS of immunocompetent recipients is highly dependent on transplantation site. *Cell Transplant.* 23, 253–262
106 Moriyama, E.H. *et al.* (2008) The influence of hypoxia on bioluminescence in luciferase-transfected gliosarcoma tumor cells *in vitro*. *Photochem. Photobiol. Sci.* 7, 675–680
107 Ueda, I. *et al.* (1976) Molecular mechanism of inhibition of firefly luminescence by local anesthetics. *Proc. Natl. Acad. Sci.* 73, 481–485
108 Keyaerts, M. *et al.* (2011) Plasma protein binding of luciferase substrates influences sensitivity and accuracy of bioluminescence imaging. *Mol. Imaging Biol.* 13, 59–66
109 Iwano, S. *et al.* (2018) Single-cell bioluminescence imaging of deep tissue in freely moving animals. *Science* 359, 935–939
110 Srinivas, M. *et al.* (2013) Cell tracking using multimodal imaging. *Contrast Media Mol. Imaging* 8, 432–438
111 Kedziorek, D.A. *et al.* (2013) Using C-arm X-ray imaging to guide local reporter probe delivery for tracking stem cell engraftment. *Theranostics* 3, 916–926
112 Guglielmetti, C. *et al.* (2014) Multimodal imaging of subventricular zone neural stem/progenitor cells in the cuprizone mouse model reveals increased neurogenic potential for the olfactory bulb pathway, but no contribution to remyelination of the corpus callosum. *Neuroimage* 86, 99–110
113 Grossmann, U. *et al.* (2014) Double-labeling of stem cells for combined brain PET/MRI. *Soc. Nucl. Med. Annu. Meeting Abstr.*
114 Lewis, C.M. *et al.* (2015) 52Mn production for PET/MRI tracking of human stem cells expressing divalent metal transporter 1 (DMT1). *Theranostics* 5, 227–239
115 Garikipati, V.N.S. *et al.* (2014) Mesenchymal stem cells from fetal heart attenuate myocardial injury after infarction: an *in vivo* serial pinhole gated SPECT-CT study in rats. *PLoS One* 9, e100982
116 Rojas, S.V. *et al.* (2017) Multimodal imaging for *in vivo* evaluation of induced pluripotent stem cells in a murine model of heart failure. *Artif. Organs* 41, 192–199
117 Harding, J. *et al.* (2013) Large animal models for stem cell therapy. *Stem Cell Res. Ther.* 4, 23
118 De Becker, A. and van Riet, I. (2016) Homing and migration of mesenchymal stromal cells: how to improve the efficacy of cell therapy? *World J. Stem Cells* 8, 73
119 Lee, R.H. *et al.* (2009) Intravenous hMSCs improve myocardial infarction in mice because cells embolized in lung are activated to secrete the anti-inflammatory protein TSG-6. *Cell Stem Cell* 5, 54–63
120 Shah, S. and Heldman, A.W. (2017) Stem cell therapy in heart failure. In *Heart Failure* (Marin-Garcia, J., ed.), pp. 727–747, Springer
121 Schrepfer, S. *et al.* (2007) Stem cell transplantation: the lung barrier. *Transpl. Proc.* 39, 573–576
122 Kean, T.J. *et al.* (2013) MSCs: delivery routes and engraftment, cell-targeting strategies, and immune modulation. *Stem Cells Int.* 2013, 732742
123 Wei, X. *et al.* (2013) Mesenchymal stem cells: a new trend for cell therapy. *Acta Pharmacol. Sin.* 34, 747–754
124 Yin, X. *et al.* (2016) Engineering stem cell organoids. *Cell Stem Cell* 18, 25–38
125 Quarta, M. *et al.* (2016) An artificial niche preserves the quiescence of muscle stem cells and enhances their therapeutic efficacy. *Nat. Biotechnol.* 34, 752–759
126 Bagó, J.R. *et al.* (2017) Tumor-homing cytotoxic human induced neural stem cells for cancer therapy. *Sci. Transl. Med.* 9 eaah6510
127 Sheng, C.C. *et al.* (2012) Current stem cell delivery methods for myocardial repair. *BioMed. Res. Int.* 2013, 547902
128 Guan, J. *et al.* (2013) Transplantation of human mesenchymal stem cells loaded on collagen scaffolds for the treatment of traumatic brain injury in rats. *Biomaterials* 34, 5937–5946
129 Uchida, S. *et al.* (2016) Treatment of spinal cord injury by an advanced cell transplantation technology using brain-derived neurotrophic factor-transfected mesenchymal stem cell spheroids. *Biomaterials* 109, 1–11
130 Nicolas, C.T. *et al.* (2017) Concise review: liver regenerative medicine: from hepatocyte transplantation to bioartificial livers and bioengineered grafts. *Stem Cells* 35, 42–50
131 Chen, C. and Hou, J. (2016) Mesenchymal stem cell-based therapy in kidney transplantation. *Stem Cell Res. Ther.* 7, 16
132 Sanganalmath, S.K. and Bolli, R. (2013) Cell therapy for heart failure. *Circ. Res.* 113, 810–834
133 Kumamaru, H. *et al.* (2012) Direct isolation and RNA-seq reveal environment-dependent properties of engrafted neural stem/progenitor cells. *Nat. Commun.* 3, 1140
134 Lan, F. *et al.* (2012) Safe genetic modification of cardiac stem cells using a site-specific integration technique. *Circulation* 126, S20–28
135 Chandrasekaran, A.P. *et al.* (2017) Genome editing: a robust technology for human stem cells. *Cell. Mol. Life Sci.* 74, 3335–3346
136 Wang, G. *et al.* (2017) Efficient, footprint-free human iPSC genome editing by consolidation of Cas9/CRISPR and piggyBac technologies. *Nat. Protoc.* 12, 88–103
137 Choi, Y.J. *et al.* (2017) 3D cell printed tissue analogues: a new platform for theranostics. *Theranostics* 7, 3118–3137
138 Muller, A.M. *et al.* (2016) Hypoxia-targeted 131I therapy of hepatocellular cancer after systemic mesenchymal stem cell-mediated sodium iodide symporter gene delivery. *Oncotarget* 7, 54795–54810
139 Cheng, S.H. *et al.* (2016) Dynamic *in vivo* SPECT imaging of neural stem cells functionalized with radiolabeled nanoparticles for tracking of glioblastoma. *J. Nucl. Med.* 57, 279–284
140 Nejadnik, H. *et al.* (2015) Magnetic resonance imaging of stem cell apoptosis in arthritic joints with a caspase activatable contrast agent. *ACS Nano* 9, 1150–1160
141 Haber, T. *et al.* (2017) Ultrasound-mediated mesenchymal stem cells transfection as a targeted cancer therapy platform. *Sci. Rep.* 7, 42046
142 Bez, M. *et al.* (2017) *In situ* bone tissue engineering via ultrasound-mediated gene delivery to endogenous progenitor cells in mini-pigs. *Sci. Transl. Med.* 9
143 Park, J.S. *et al.* (2017) Multimodal magnetic nanoclusters for gene delivery, directed migration, and tracking of stem cells. *Adv. Funct. Mater.* 27
144 Park, J.S. *et al.* (2017) Multi-functional nanotracers for image-guided stem cell gene therapy. *Nanoscale* 9, 4665–4676